

Red Emitting Cerium(III) and Versatile Luminescence Chromaticity of 1D-Coordination Polymers and Heterobimetallic Ln/AE Pyridylpyrazolate Complexes

Heba Youssef,^[a, b] Jonathan Becker,^[a] Alexander E. Sedykh,^[a] Thomas Schäfer,^[a] Ilya V. Taydakov,^[c] and Klaus Müller-Buschbaum^{*[a, d]}

Dedicated to the late Professor Rudolf Hoppe on the occasion of his 100th birthday

Ten homoleptic lanthanide containing 1D-coordination polymers, three heterobimetallic lanthanide/alkaline earth complexes as well as two alkaline earth complexes of the formula $[\text{Ln}(\text{2-PyPz})_3]$, $[\text{Tb}_2\text{AE}(\text{2-PyPz})_8]$, and $[\text{AE}(\text{2-PyPz})_2(\text{2-PyPzH})_2]$, Ln=La–Nd, Sm–Ho, AE=Ca, Sr, Ba were obtained by reactions of the lanthanide (Ln) and/or the alkaline earth metals (AE) with the ligand 3-(2-pyridyl)pyrazole. Organic melt based and/or solvothermal synthesis results in a redox reaction. The investigated compounds exhibit fair thermal stability up to 400 °C. The Ce^{3+} compound exhibits a bright and red 5d-based broad

band emission with a maximum at around 640 nm under UV excitation marking an example of a strong reduction of the excited 5d states of Ce(III). The co-doping of the Gd-containing coordination polymers with Eu^{3+} and Tb^{3+} allows for a shift in the chromaticity from the ion specific 4f-based emission colors close to white light emission and thus for a versatile tuning of the chromaticity. The co-doping of Eu^{3+} with Tb^{3+} and vice versa shows metal-to-metal energy transfer (MMET) between 4f-levels of Tb^{3+} and Eu^{3+} , which influences the tuning of the emission colour.

Introduction

High intensity, low electricity consumption, and long lifetime are the advantages of solid state lighting (SSL) which is expected to replace incandescent lamps.^[1] The Ce^{3+} -doped yellow-emitting phosphor ceramic $\text{Y}_3\text{Al}_5\text{O}_{12}$ can be effectively excited by a blue-emitting laser and used in higher-power white light applications due to its high luminescent efficiency and

thermal stability.^[2] Also, Ce^{3+} containing coordination polymers and complexes have short excited-state lifetimes (< 100 ns)^[3] ascribed to the beneficial character of the spin- and parity-allowed d-f transitions.^[4] Ce^{3+} allows for a tunable emission color, because the excited 5d energy levels are sensitive to the coordination environment, resulting in dependence of the coordination partners and the crystal field on the emission and its chromaticity.^[5] The cost of cerium is rather low due to its abundance on Earth (higher than copper) and a less complicated isolation process from other lanthanide elements.^[4b,6] Most reported Ce^{3+} complexes are non-emissive due to luminescence quenching by linkers and solvent molecules.^[7] The emissive Ce^{3+} examples in the literature are mainly near UV and blue emitters^[8] beside some doped materials exhibiting green/yellow^[9] or even the unusual yellow emission.^[10] Recently, the red emission in solid state LEDs was within the scope of Ce/Pr systems, such as $\text{Lu}_3\text{Al}_5\text{O}_{12}:\text{Ce}^{3+}\text{Pr}^{3+}$,^[11] $\text{YAG}:\text{Ce}^{3+}\text{Pr}^{3+}$,^[12] $\text{Gd}_3\text{Ga}_5\text{O}_{12}:\text{Ce}^{3+}\text{Pr}^{3+}$,^[13] $\text{Y}_3\text{Al}_5\text{O}_{12}:\text{Ce}$ nanophosphor doped with Pr^{3+} ,^[14] and the cerium-doped scandate.^[15] We now present an undoped Ce^{3+} red phosphor, which indicates the value of investigating new N-donor based ligands and coordination compounds to achieve a high variety of photoluminescence of the lanthanides.

Heterobimetallic terbium/alkaline earth (Tb/AE) compounds reported in the literature contain either oxygen donors or multifunctional donors,^[16] such as $[\text{Tb}_2\text{Ca}(\text{OQ})_8] \cdot n\text{HOQ}$ (OQ = 8-quinolate).^[17] Fewer examples are known for the bimetallic system Tb/Sr, e.g. $[\text{Tb}_2\text{Sr}_3(\text{pda})_6(\text{H}_2\text{O})_{18}] \cdot 13\text{H}_2\text{O}$.^[18]

Previously, the ligand 3-(2-pyridyl)pyrazole (2-PyPzH) was mainly used in the synthesis of transition-metal complexes and CPs, either as the main reacting ligand^[19] or as a co-ligand,^[20] such as the formation of 2D open-channel cadmium(II) frame-

[a] H. Youssef, Dr. J. Becker, A. E. Sedykh, T. Schäfer, Prof. Dr. K. Müller-Buschbaum

Institute of Inorganic and Analytical Chemistry
Justus-Liebig-University Giessen

Heinrich-Buff-Ring 17, 35392 Giessen, Germany

E-mail: klaus.mueller-buschbaum@anorg.chemie.uni-giessen.de

[b] H. Youssef

Department of Chemistry

Faculty of Science, Mansoura University

El Gomhouria, Mansoura Qism 2, 11432, Mansoura Dakahlia Governorate, (Egypt)

[c] Prof. Dr. I. V. Taydakov

Lebedev Physical Institute of the Russian Academy of Sciences

Leninskiy pr-t, 53, 119991, Moscow, Russia

[d] Prof. Dr. K. Müller-Buschbaum

Center of Materials Research (LAMA)

Justus-Liebig-University Giessen

Heinrich-Buff-Ring 16, 35392 Giessen, Germany



Supporting information for this article is available on the WWW under <https://doi.org/10.1002/zaac.202200295>



© 2022 The Authors. Zeitschrift für anorganische und allgemeine Chemie published by Wiley-VCH GmbH. This is an open access article under the terms of the Creative Commons Attribution Non-Commercial License, which permits use, distribution and reproduction in any medium, provided the original work is properly cited and is not used for commercial purposes.

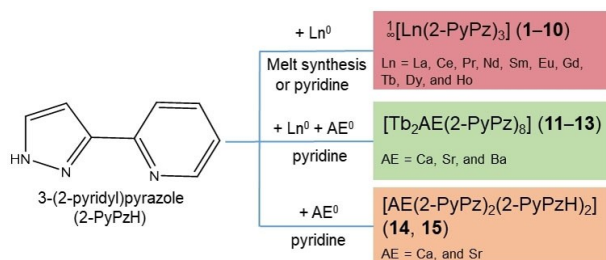
works using the mixed ligands terephthalic acid and 2-PyPzH.^[21] The tridentate ligand was previously reacted with Ln(NO₃)₃·6H₂O, Ln=Eu³⁺, Sm³⁺ using ethanol as solvent to obtain complexes, for a selective extraction of actinides over [Eu(PyPzH)₂(NO₃)₃].^[22] To the best of our knowledge, the ligand 2-PyPzH has not yet been used in reactions with a heterobimetallic AE/Ln system, nor monometallic AE. Instead, 2-PyPzH was used as a starting material in a large number of ligand syntheses. Some of these derivatized ligands were later used in coordination chemistry with transition metals^[23] and lanthanides,^[24] as well as a few examples with AE metals.^[25] Related ligands, such as 3-(3-pyridyl)pyrazole (3-PyPzH), and 3-(4-pyridyl)pyrazole (4-PyPzH), have been used to obtain Cu⁺ and Ag⁺ complexes, indicating a high-lying intersystem crossing that can lead to efficient phosphorescence.^[26] Besides, homoleptic and highly luminescent trivalent lanthanide 3D coordination polymers with the formulas ³∞[Ln(3-PyPz)₃], and ³∞[Ln(4-PyPz)₃], Ln=Sm, Eu, Gd, Tb, Dy were recently investigated in our group.^[27] Based on these results, we successfully attempted to synthesize new luminescent coordination polymers along the lanthanide series, homoleptic, heterobimetallic rare earth/alkaline earth compounds.

Results and Discussion

Synthesis and Structural Analysis

Either organic melt or solvothermal synthesis-based reactions of 3-(2-pyridyl)pyrazole (2-PyPzH) (Scheme 1) with elemental lanthanides were used to obtain a series of ten coordination polymers ¹∞[Ln(2-PyPz)₃], Ln=La (1), Ce (2), Pr (3), Nd (4), Sm (5), Eu (6), Gd (7), Tb (8), Dy (9), and Ho (10). Solvothermal reactions of 2-PyPzH with a mixture of elemental Tb and AE yielded three complexes [Tb₂AE(2-PyPz)₈], AE=Ca (11), Sr (12), and Ba (13), while the reaction with elemental alkaline earth metal obtained two complexes [AE(2-PyPz)₂(2-PyPzH)₂], AE=Ca (14), and Sr (15).

All synthesized compounds crystallize in the monoclinic crystal system, ¹∞[Ln(2-PyPz)₃], Ln=La–Ho (1–10) in *P*₂₁, [Tb₂AE(2-PyPz)₈], AE=Ca (11), Ba (13) and [Sr(2-PyPz)₂(2-PyPzH)₂] (15) in *P*₂₁/*n*, and [Ca(2-PyPz)₂(2-PyPzH)₂] (14) in *C*2/*c*, except for [Tb₂Ca(2-PyPz)₈] (11), which crystallizes in the triclinic crystal



Scheme 1. Synthetic scheme for reactions with 2-PyPzH to obtain the presented 15 compounds: 1D-coordination polymers (top), bimetallic complexes (center), and alkaline earth-based complexes (bottom).

system with space group *P*–1. In ¹∞[Ln(2-PyPz)₃] (1–10), each Ln³⁺ ion coordinates to nine nitrogen atoms in a distorted tricapped trigonal fashion, two nitrogen atoms of the pyrazolate anion acting as a bridge between two neighboring trivalent lanthanide ions, resulting in an altogether one-dimensional coordination polymer (Figure 1a, 1b). The coordination environment of Tb³⁺ decreases to eight when AE²⁺ is added to the heterobimetallic system [Tb₂AE(2-PyPz)₈] (11–13) forming a distorted bi-capped trigonal prism (Figure 1c, 1d). The higher tendency of Ln³⁺ to form high coordination numbers drives Tb³⁺ to allocate a position, in which it can coordinate with two nitrogen atoms of both, the pyridyl ring and the pyrazolate ring of each tridentate ligand, so that each rare earth ion binds to three chelating bridging ligands and a terminal pyridylpyrazolate anion. These ligands bridge through the pyrazolate ring to the central hexacoordinated alkaline earth atom in a distorted tetragonal bipyramidal environment. The absence of Ln³⁺ in the [AE(2-PyPz)₂(2-PyPzH)₂] complexes allows the AE²⁺ ions to occupy a central position to coordinate with eight nitrogen atoms leading to a higher coordination number of AE compared to the bimetallic complexes, and each ligand acts as a bidentate chelating Lewis base (Figure 1e, 1f). Electroneutrality is settled by two protons bridging two pyrazolate moieties with two neutral ligands. The backbones of the two pyridylpyrazolate units are perpendicular to each other, resulting in a triangular dodecahedron as coordination polyhedron. The larger ionic radius of eight-coordinate AE²⁺ in the monometallic complexes [AE(2-PyPz)₂(2-PyPzH)₂], AE=Ca (14), and Ba (15) leads to a general elongation of the Ca–N(pz) distance, N(pz) being the pyrazolate nitrogen atom, compared to the heterobimetallic complexes [Tb₂AE(2-PyPz)₈], AE=Ca (11), and Sr (12), in which AE²⁺ is six-coordinate. The average Ca–N(pz) distance in 11, and 12 is 253 pm, while in 14, and 15, it is 258 pm. This corresponds well with the change in the ionic radius of AE²⁺ as does the increase in the AE–N distances from an average of 244 in 11 to 280 pm in 13 for the AE²⁺ ions Ca²⁺ and Sr²⁺. Similar trinuclear complexes with homoleptic nitrogen donor Lewis base could not be found in the literature, so we compare the average of Ca–N(pz) (244 pm, 11), and Sr–N(pz) (262 pm, 12) with a mononuclear system, such as AE bis[κ³N–tris(3,4,5-trimethylpyrazolyl)methanide] (Ca–N 244.1, Sr–N 258.3 pm),^[28] revealing good agreement. For 15, the average of Sr–N(py) (273 pm), N(py) being the pyridyl nitrogen atom are larger than the corresponding average of the Sr–N of the pyrazolate rings (Sr–N(pz) 264 pm) as a result of larger electrostatic attraction. In addition, the Sr1–N(py) distances (274.0(2) pm), and Sr2–N(py) (271.4(3) pm) of the deprotonated ligands are shorter than to the pyridyl groups of the neutral ligands (271.7(2), and 272.6(2) pm). Good agreement of the Sr–N distances is observed between 15 (263.2(2)–277.9(3) pm) and the strontium complex bis[3-(1-naphthyl)-5-(2-pyridyl)-2H-pyrazole]strontium bis[3-(1-naphthyl)-5-(2-pyridyl)pyrazolate] (263.8–276.3 pm) with slightly smaller values for the anionic pyrazolate anions.^[25b] The interatomic distances of the pyridylpyrazolate anions and the neutral pyridylpyrazolate molecules are similar (Table S5), indicating aromatic character in all eight pyridylpyrazolate units, supporting the highly acidic character

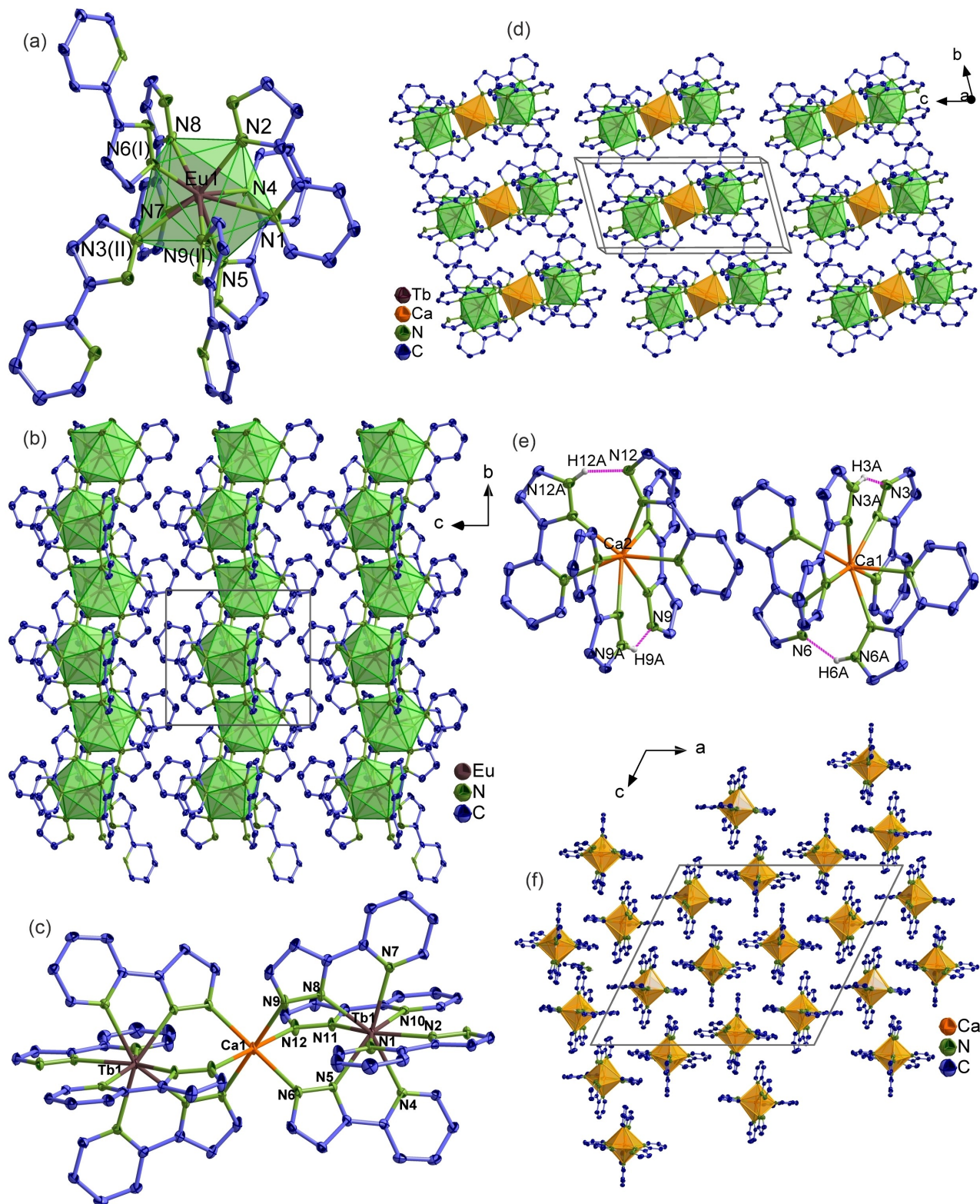


Figure 1. (a) Extended coordination sphere of Eu^{3+} in $[\text{Eu}(\text{2-PyPzH})_3]$ (6), representing the series of isotopic one-dimensional coordination polymers (1–10). (b) Exemplary crystal structure of 6 with a view along [100]. (c), (d) Excerpts of the crystal structure and view of the unit cell of $[\text{Tb}_2\text{Ca}(\text{2-PyPz})_8]$ (11). (e), (f) Excerpts of the crystal structure and unit cell of $[\text{Ca}(\text{2-PyPz})_2(\text{2-PyPzH})_2]$ (14) with a view along [010]. N...H...N hydrogen bridges are indicated by dashed lines, the polyhedra around Ln^{3+} , and Ca^{2+} are indicated in green, and orange, respectively. Hydrogen atoms are omitted for clarity, and the thermal ellipsoids are depicted at a 50% probability level for all structures. Symmetry operations: I = $-x + 2, y + 1/2, -z + 1$ II = $-x + 2, y - 1/2, -z + 1$.

of the bridging hydrogen atoms. No delocalization of the negative charge of the pyrazolate moieties to the outer aromatic rings is obvious from interatomic distances.

All bulk products (1–15) were investigated by PXRD (Figure 2, S4, S5). The experimental diffraction patterns agree with the diffraction patterns simulated from single-crystal data for all investigated compounds, taking into account the possibility of the first two reflections in $1_{\infty}[\text{Ln}(\text{2-PyPzH})_3]$ (1–10) to merge and appear as one reflection (Figure S3). Since the lengths of the a -axis (1114.7 pm) and the c -axis (1130.1 pm) are close, the spacing of the lattice planes d_{hkl} for [001] and [100], representing the first ($2\theta = 8.786^\circ$) and the second reflection ($2\theta = 8.907^\circ$), respectively, is low. With less than 14 pm between the two lattice planes, the expansion of the volume of the unit cell and the lattice parameters due to the increase in the ionic radii from Ho^{3+} to La^{3+} , and contractions of the angles, one merged broader reflection can be expected to be observed instead of the previously discussed two reflections.

Photophysical Properties

UV-Vis-NIR absorption spectra

Electronic absorption spectra as well as excitation and emission spectra were recorded in the solid state to allow photophysical interpretations of the products $1_{\infty}[\text{Ln}(\text{2-PyPz})_3]$, $\text{Ln} = \text{La}$ (1), Ce (2), Pr (3), Nd (4), Sm (5), Eu (6), Tb (8), Dy (9), Ho (10), and $[\text{Tb}_2\text{AE}(\text{2-PyPz})_8]$ (11–13) at room temperature (Figure 3). Absorption spectra localized to the ligand moieties of the Ln^{3+} -based compounds have been reported in the literature and were mostly studied in solution,^[29] whereas fewer examples of lanthanide nitrate-based compounds have been reported for the solid state for a wavelength range not exceeding 1000 nm.^[30] The absorption spectrum for 2-PyPZH was shown in the literature for the solid state and in acetonitrile solution ($7.8 \times 10^{-5} \text{ mol L}^{-1}$) where two characteristic K-band (ca. 210–265 nm; $47619 \sim 37736 \text{ cm}^{-1}$) and B-band (285–350 nm; $35088 \sim 28571 \text{ cm}^{-1}$) regions corresponding to the $\pi \rightarrow \pi^*$ transitions were observed.^[20,31] In the products presented here, an intense wide absorption band of the ligand in the UV region due to coordination appears for every sample, as shown in Figure 3. In addition, sharp and weak to medium bands can be assigned to the respective f–f transitions in both VIS and NIR regions for $1_{\infty}[\text{Ln}(\text{2-PyPz})_3]$, $\text{Ln} = \text{Pr}^{3+}$ (3), Nd^{3+} (4), Sm^{3+} (5), Dy^{3+} (9), and Ho^{3+} (10) ions, as assigned in Table 1.^[30d,32] For $1_{\infty}[\text{Ce}(\text{2-PyPz})_3]$ (2), formation of a shoulder at a higher wavelength is observed due to transition from 4f to 5d. The addition of alkaline earth ions to Tb^{3+} led to the formation of a new broad absorption band starting at 515 nm (19417 cm^{-1}) in $[\text{Tb}_2\text{Ca}(\text{2-PyPz})_8]$ (11) and 470 nm (21277 cm^{-1}) in $[\text{Tb}_2\text{Sr}(\text{2-PyPz})_8]$ (12) with maxima at 583 and 532 nm (17153 and 18797 cm^{-1}), respectively, and at 480 nm (20833 cm^{-1}) for $[\text{Tb}_2\text{Ba}(\text{2-PyPz})_8]$ (13) being less distinguishable between two maxima.

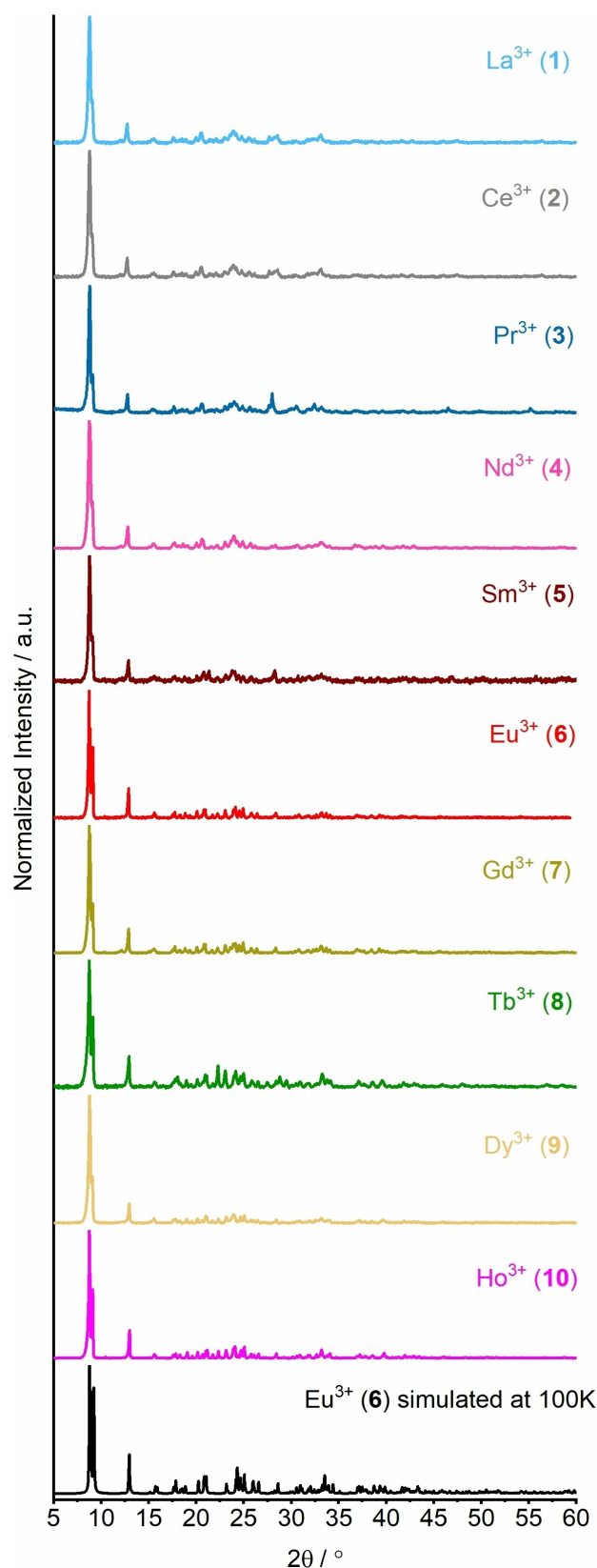


Figure 2. Comparison of the experimental X-ray powder diffraction patterns of $1_{\infty}[\text{Ln}(\text{2-PyPz})_3]$, $\text{Ln} = \text{La}$ (1), Ce (2), Pr (3), Nd (4), Sm (5), Eu (6), Gd (7), Tb (8), Dy (9), Ho (10) at 298 K with the respective simulated pattern from single-crystal X-ray data at 100 K.

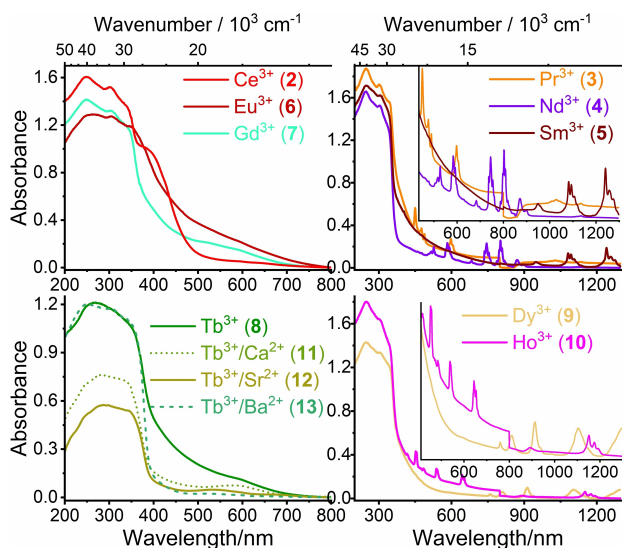


Figure 3. Solid state absorption spectra of $^1_{\infty}[\text{Ln}(\text{2-PyPz})_3]$, $\text{Ln}=\text{Ce}^{3+}$ (2), Pr^{3+} (3), Nd^{3+} (4), Sm^{3+} (5), Eu^{3+} (6), Gd^{3+} (7), Tb^{3+} (8), Dy^{3+} (9), Ho^{3+} (10) and $[\text{Tb}_2\text{AE}(\text{2-PyPz})_8]$, $\text{AE}=\text{Ca}$ (11), Sr (12), and Ba (13) in the solid state at room temperature.

Emission and excitation spectra

The one-dimensional coordination polymer $^1_{\infty}[\text{Ce}(\text{2-PyPz})_3]$ (2) shows interesting photoluminescence properties with Ce^{3+} -centered emission in the VIS range of red color, which can already be seen with the naked eye under the UV lamp. Photoluminescence spectroscopy determinations of 2 (Figure 4) reveal broadband emission from 500 to exceed 850 nm being centered at 640 and 620 nm (15625 and 16129 cm^{-1}) for 77 K and RT, respectively, and indicating large crystal field splitting and a large redshift for the emission wavelength of Ce^{3+} . The excitation spectrum exhibits a shoulder at 392 nm (25510 cm^{-1}) at 77 K, and 379 nm (26385 cm^{-1}) at RT, which correspond to the lowest energy levels of the crystal field splitting bands of the 5d excited state of the Ce^{3+} ion. The maximum excitation band at 335 nm (29851 cm^{-1}) is correlated with the coordinated 2-PyPzH ligand. The lifetime of 2 is only 2 ns as a result of the parity allowed nature of the 5d–4f transition. Actually, red-emitting cerium in 2 has a shorter lifetime than the reported yellow, blue, and green Ce^{3+} emitters, being on the order of tens of nanoseconds.^[3a,b] For instance, the mixed ligand series of the luminescent Ce^{3+} complex with the general one formula $[(\text{Me}_3\text{Si})_2\text{NC}-(\text{NiPr})_2]_x\text{Ce}[\text{N}(\text{SiMe}_3)_2]_{3-x}$ ($x=0$, 1-N; $x=1$, 2-N; $x=2$,

3-N; $x=3$, 4) that exhibit yellow (1-N), lime-green (2-N), green (3-N), and blue light (4) emission with lifetimes of 24, 65, 117, and 83 ns, respectively.^[5d] In contrast, distinct longer lifetimes are observed for the parity-forbidden 4f–4f transitions, which reach the microsecond scale for Sm^{3+} , Eu^{3+} , Tb^{3+} , and Dy^{3+} (Table 2). A considerable antenna effect is expected for both Eu^{3+} (6), and Tb^{3+} (8), with the ligand being mainly responsible for the excitation. For Pr^{3+} (3), Nd^{3+} (4), Sm^{3+} (5), and Dy^{3+} (9), additional weak direct 4f–4f-excitation is indicated by a series of low intensities of ion-specific sharp lines (Figures 4, 5). As a result of the energy differences (ΔE) between the ligand triplet state ($\sim 22831\text{ cm}^{-1}$) and the energy positions of Eu^{3+} ($^5D_0=20100\text{ cm}^{-1}$), and Tb^{3+} ($^5D_4=20500\text{ cm}^{-1}$)^[32a,c] considering the Latva rule, ΔE is 2731, and 2331, respectively. Thereby, the ΔE value is in the optimal range ($2500\text{--}3000\text{ cm}^{-1}$) in Eu^{3+} and still close enough for Tb^{3+} . Thus, it is expected that the Eu^{3+} , Tb^{3+} based compounds would have the highest lifetime and quantum yield among the series. This conclusion is supported by the observation of long lifetimes for Eu^{3+} (6) emissive state (870 μs), and Tb^{3+} (8) (280 μs) in comparison to Sm^{3+} (5) (8.28 μs), and Dy^{3+} (9) (4.14 μs).

In addition, the observed quantum yield (QY) is found to be highest for the Eu^{3+} , and Tb^{3+} coordination polymers 6, and 8, although it is altogether limited, with $\text{QY}=5.8(4)$, and $6.3(5)\%$, respectively. Notably, the triplet state of the ligand was revealed by the emission of the Gd^{3+} containing compound, a phosphorescence band with onset at $\lambda_{\text{onset}}=438\text{ nm}$ (22831 cm^{-1}) being intense and better resolved at 77 K. The phosphorescent emission was also detected with a gating (cutting off the emission of the singlet state, Figure S13). The photophysical properties of the obtained products with Sm^{3+} (5), Eu^{3+} (6), Tb^{3+} (8), and Dy^{3+} (9) are comparable to homoleptic frameworks with 3-(3-pyridyl)pyrazolate (3-PyPz $^-$), and 3-(4-pyridyl)pyrazole (4-PyPz $^-$). The longer lifetime observed for Eu^{3+} (870 μs) and the shorter lifetime for Tb^{3+} (8) (280 μs) in comparison to those reported for the $^3_{\infty}[\text{Ln}(\text{3-PyPz})_3]$, ($\text{Ln}=\text{Eu}$ (576 μs), and Tb (1087.4 μs), and $^3_{\infty}[\text{Ln}(\text{4-PyPz})_3]$ ($\text{Ln}=\text{Eu}$ (323 μs), Tb (627.3 μs)^[27] is related to the position of the triplet state for 3-PyPz $^-$ ($\lambda_{\text{onset}}=430\text{ nm}$, $\sim 23250\text{ cm}^{-1}$) and 4-PyPz $^-$ ($\lambda_{\text{onset}}=423\text{ nm}$, $\sim 23640\text{ cm}^{-1}$). This leads to a better energy transfer to Tb^{3+} and less for Eu^{3+} excited 4f states. The lifetimes for Sm^{3+} (5), and Dy^{3+} (9) are shorter than for $^3_{\infty}[\text{Ln}(\text{3-PyPz})_3]$, ($\text{Ln}=\text{Sm}$ (15.9 μs), and Dy (15.7 μs), and $^3_{\infty}[\text{Ln}(\text{4-PyPz})_3]$ ($\text{Ln}=\text{Sm}$ (15.8 μs), Dy (12.1 μs). However, the lifetimes for Sm^{3+} (5), Tb^{3+} (8), and Dy^{3+} (9) are still higher than several examples in the literature.^[33] The internal quantum yield (IQY) of the Eu^{3+} centered emission was calculated using Wert's formula with

Table 1. Absorption wavelengths of transitions of $^1_{\infty}[\text{Ln}(\text{2-PyPz})_3]$, $\text{Ln}=\text{Pr}$, Nd , Sm , Dy , and Ho in the solid state at room temperature.

Intra-4f absorption transitions			
	Ground state	Excited states	
Pr^{3+} (3)	$^3H_4 \rightarrow$	$^3P_2, ^3P_1, ^3P_0, ^1D_2$	450, 476, 489, 597 nm
Nd^{3+} (4)	$^4I_{9/2} \rightarrow$	$^4G_{7/2}, ^4G_{5/2}, ^4F_{9/2}, ^4F_{7/2}, ^4F_{5/2}, ^4F_{3/2}$	527, 583, 683, 745, 802, 871 nm
Sm^{3+} (5)	$^6H_{5/2} \rightarrow$	$^6F_{11/2}, ^6F_{9/2}, ^6F_{7/2}$	949, 1081, 1240 nm
Dy^{3+} (9)	$^6H_{15/2} \rightarrow$	$^6F_{3/2}, ^6F_{5/2}, ^6F_{7/2}, ^6F_{9/2}$	760, 810, 913, 1104 nm
Ho^{3+} (10)	$^5I_8 \rightarrow$	$(^5G, ^3G)_5, ^5G_6, ^5F_3, ^5F_4, ^5F_5, ^5I_6$	417, 452, 484, 538, 644, 1151 nm

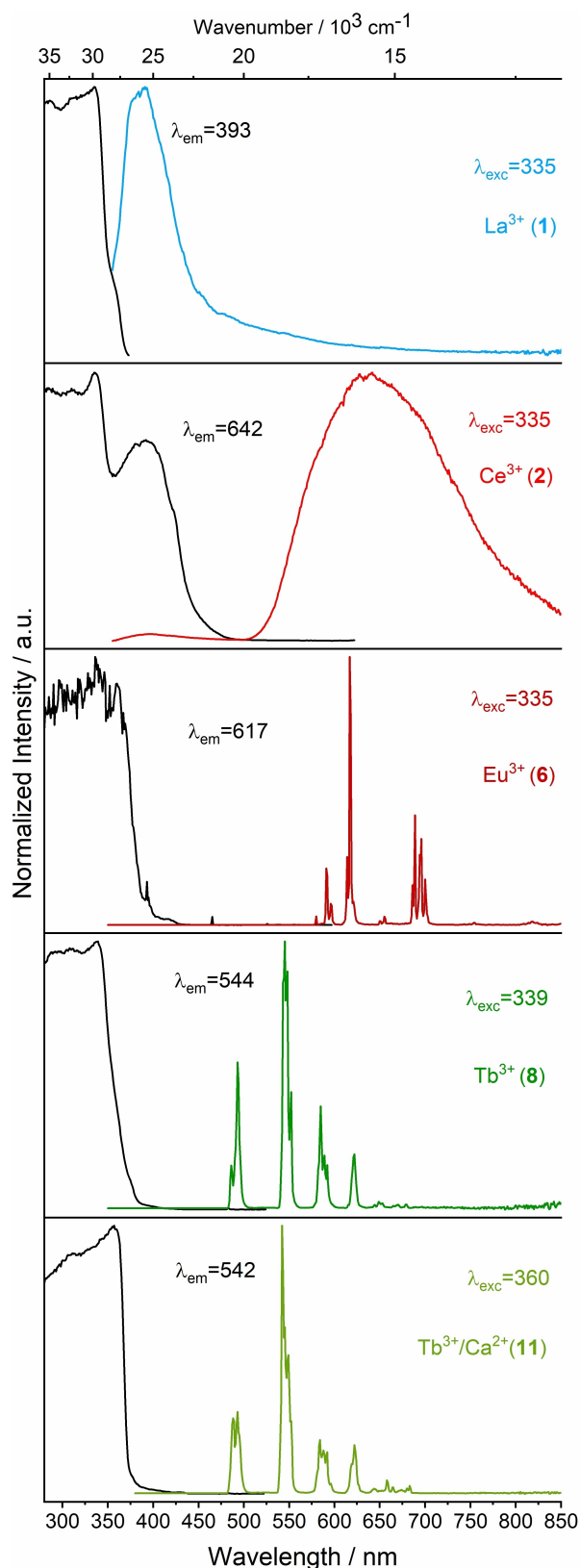


Figure 4. Normalized solid state excitation (black) and emission (colored) spectra of ${}^1\infty[\text{Ln}(2\text{-PyPz})_3]$, $\text{Ln}=\text{La}$ (1), Ce (2), Eu (6), and Tb (8) as well as $[\text{Tb}_2\text{Ca}(2\text{-PyPz})_8]$ (11) at 77 K. Wavelengths for which the spectra were recorded are reported in the legends.

refractive index equals 1.5.^[34] The equation gives a moderate-high Internal QY of 37.2 % which is in the middle of ${}^3\infty[\text{Eu}(3\text{-PyPz})_3]$ and ${}^3\infty[\text{Eu}(4\text{-PyPz})_3]$ 48 and 33%, respectively.

The excitation spectra for 2-PyPzH at RT and 77 K show broadband in the UV region with maxima at 364 nm (27472 cm^{-1}) corresponding to the $\text{S}_n \leftarrow \text{S}_0$ transitions.^[19c,20g,i] This ligand-based excitation band shows a hypochromic shift upon coordination to the investigated compounds (1–11). The emission maxima of the ligand are observed in the range of 400 to 410 nm (25000 to 24390 cm^{-1}), as reported.^[19c,20g,i] This fluorescence band has a lifetime of 1.47(7) ns, which is shorter than the related ligands 3-PyPzH (3.4 ns), and 4-PyPzH (6.07 ns).^[27]

For ${}^1\infty[\text{Eu}(2\text{-PyPz})_3]$ (6) and ${}^1\infty[\text{Tb}(2\text{-PyPz})_3]$ (8) (Figure 4), the highest intensity is found for the transitions ${}^5\text{D}_0 \rightarrow {}^7\text{F}_2$ at 517 nm (19342 cm^{-1}), and ${}^5\text{D}_4 \rightarrow {}^7\text{F}_5$ at 545 nm (18349 cm^{-1}), respectively, as expected for Eu^{3+} and Tb^{3+} .^[35] For 6, the transition ${}^5\text{D}_0 \rightarrow {}^7\text{F}_0$ indicates that the Eu^{3+} ion occupies a site of the C_{nv} , C_n , or C_s symmetry class (in this particular case C_3), to evade the selection rules of the Judd-Ofelt theory.^[35a]

The emission spectra of $[\text{Tb}_2\text{AE}(2\text{-PyPz})_8]$ (11–13) display rather sharp lines, which can be identified with f–f transitions regarding Tb^{3+} between the ${}^5\text{D}_4$ excited state and the ${}^7\text{F}_{6-0}$ levels. Ligand emission is also observable at RT for $[\text{Tb}_2\text{Ca}(2\text{-PyPz})_8]$ (11), and $[\text{Tb}_2\text{Sr}(2\text{-PyPz})_8]$ (12), exhibiting a hypochromic shift caused by a decrease in the π -electron density of the pyridylpyrazolate anions by the double linkage to two metal ions. For ${}^1\infty[\text{Pr}(2\text{-PyPz})_3]$ (3), ${}^1\infty[\text{Sm}(2\text{-PyPz})_3]$ (5), and ${}^1\infty[\text{Dy}(2\text{-PyPz})_3]$ (9) (Figure 5), the highest intensity is found at 617 (16207 cm^{-1} , for Pr^{3+} , corresponding to ${}^3\text{P}_0 \rightarrow {}^3\text{H}_6$), 598 (16722 cm^{-1} , for Sm^{3+} , corresponding to ${}^4\text{G}_{5/2} \rightarrow {}^6\text{H}_{7/2}$), and 572 nm (17482 cm^{-1} , for Dy^{3+} , corresponding to ${}^4\text{F}_{9/2} \rightarrow {}^6\text{H}_{13/2}$), respectively. NIR emission bands can also be observed for 3 at 1045 nm (9569 cm^{-1}) corresponding to ${}^1\text{D}_2 \rightarrow {}^3\text{F}_4$ transition of Pr^{3+} , for 5 at 782, 898, 945, 1025, and 1172 nm (12788, 11136, 10582, 9756, and 8532 cm^{-1}) corresponding to the ${}^4\text{G}_{5/2} \rightarrow {}^6\text{H}_{13/2}$ and ${}^4\text{G}_{5/2} \rightarrow {}^6\text{F}_{J/2}$, $J=3-9$ transitions of Sm^{3+} and for 9 at 750, 849, 948, 1008, 1170, and 1288 nm (13333, 11779, 10548, 9921, 8547, and 7764 cm^{-1}) corresponding to the transitions ${}^4\text{F}_{9/2} \rightarrow {}^6\text{H}_{J/2}$, ($J=9, 7, 5$), and ${}^6\text{F}_{J/2}$, ($J=7, 5, 3$) of Dy^{3+} , respectively. NIR emission bands can also be observed for Nd^{3+} (4), and Ho^{3+} (10) at 900, 1063, and 1370 nm (11111, 9407, and 7299 cm^{-1}) corresponding to ${}^4\text{F}_{3/2} \rightarrow {}^4\text{I}_{J/2}$, ($J=9, 11, 13$) transitions of Nd^{3+} ions and for 10 at 985, 1186 nm (10152, 8432 cm^{-1}) corresponding to ${}^5\text{F}_5 \rightarrow {}^5\text{I}_7$ and ${}^5\text{I}_6 \rightarrow {}^5\text{I}_8$ transitions beside the VIS transition at 656 nm (15244 cm^{-1}) corresponding to ${}^5\text{F}_5 \rightarrow {}^5\text{I}_8$ of Ho^{3+} , respectively.

Tuning of the luminescence chromaticity is further possible by co-doping of several of the products with Tb^{3+} and/or Eu^{3+} , including the Ce-based emitter. Deliberate co-doping of the Ce-containing coordination polymer with 0.5% Tb^{3+} already shifts the emission color towards a higher energy region, this shift continues with the statistic replacement of Ce^{3+} by 5% Tb^{3+} (Figure S21). The Ce emission in the co-doped samples is partly quenched and an enhancement of the Tb emission observed.

This can be attributed to the fact that Ce^{3+} is a sensitizer due to its allowed f–d transitions and its broad emission band

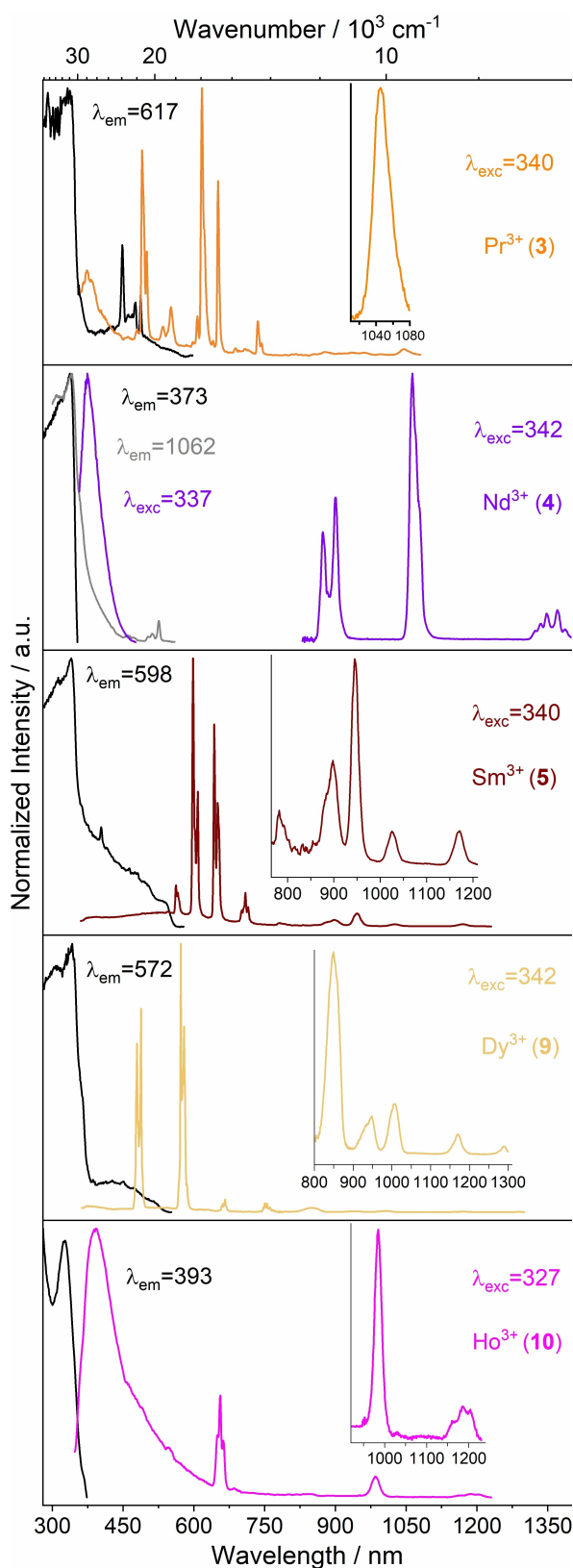


Figure 5. Normalized solid state excitation (black) and emission spectra (colored) of ${}^{\infty}[\text{Ln}(\text{2-PyPz})_3]$, Ln=Pr (3), Nd (4), Sm (5), Dy (9), and Ho (10) at 77 K. Wavelengths, for which the spectra were recorded, are reported in the legends.

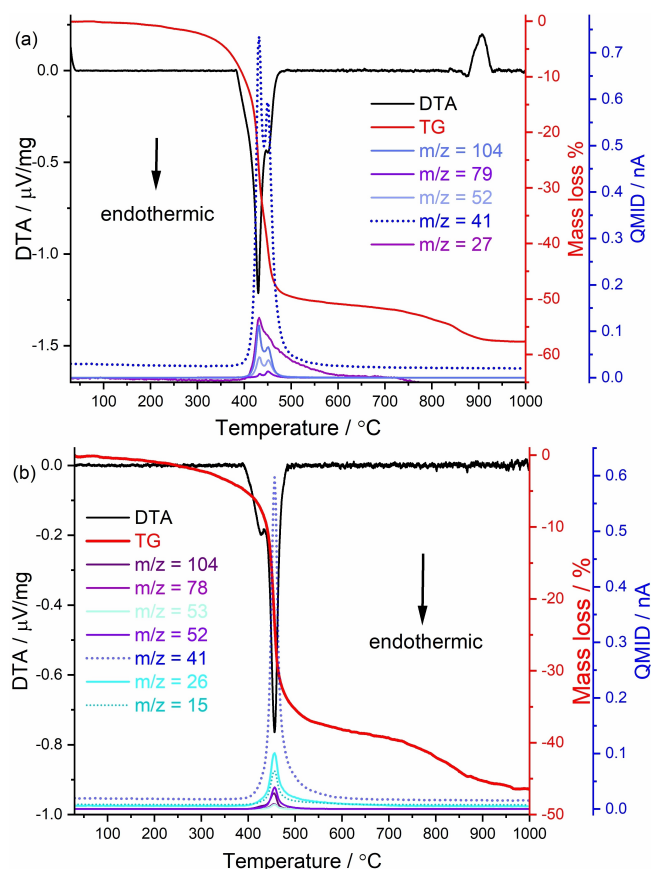


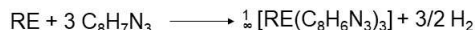
Figure 6. Simultaneous DTA/TG analysis together with mass spectrometry of ${}^{\infty}[\text{Eu}(\text{2-PyPz})_3]$ (6) representing the series of isotopic compounds (1–10) (a) and $[\text{Tb}_2\text{Ca}(\text{2-PyPz})_3]$ (11) (b). The investigation was performed in a constant flow of argon of $50 \text{ ml} \cdot \text{min}^{-1}$ with a heating rate of $5 \text{ K} \cdot \text{min}^{-1}$ from room temperature to 1000°C .

PyPzH) $_2$] have also been obtained. The Ln^{3+} ions exhibit a change in coordination number from nine to eight and the AE^{2+} ions from six to eight upon the change between monometallic and bimetallic products. SC and PXRD, elemental analysis, IR as well as photoluminescence spectroscopy, and thermal analysis led to characterization of the new compounds. The luminescence of the other products is dominated by ion specific Ln-based 4f–4f transitions from this VIS to the NIR range benefitting from a strong sensitizing effect of the ligand. Tuning of the luminescence chromaticity is further possible by co-doping several of the products including the Ce-based emitter with Tb^{3+} and/or Eu^{3+} . The co-doping of the Gd-containing coordination polymer with Eu^{3+} and Tb^{3+} allows tuning towards white-light emission. Altogether, this shows the high potential of coordination polymers together with pyridylpyrazolate ligands as N-donors for versatile photoluminescence properties.

Experimental Section

Synthesis and Analytical Data

Reactions of the different lanthanide and/or alkaline earth metals with the aromatic N-heterocyclic ligand 3-(2-pyridyl)pyrazole (2-PyPzH) proceed by a redox reaction yielding hydrogen:



Deposition Numbers 2204784 (for **6**), 2204790 (for **11**), 2204792 (for **12**), 2204788 (for **13**), 2204791 (for **14**), 2204789 (for **15**), contain the supplementary crystallographic data for this paper. These data are provided free of charge by the joint Cambridge Crystallographic Data Centre and Fachinformationszentrum Karlsruhe.

General Information: All syntheses involving lanthanide and alkaline earth elements were performed under argon or using vacuum lines, gloveboxes (MBraun Labmaster SP, Innovative Technology PureLab), Schlenk tubes, and Duran® glass ampoules (outer Ø 10 mm, wall thickness 1.5 mm). Pyridine and dichloromethane were purified by distillation and dried by standard procedures or used from the solvent purification system SPS-800 by MBraun (Garching, Germany). The bulk materials were characterized by both powder X-ray diffraction (PXRD) as well as CHN analysis.

Starting Materials: 3-(2-pyridyl)pyrazole (2-PyPzH) was synthesized as reported in the literature.^[38] The method is described in detail in the Supporting Information. Lanthanide metals (gadolinium: 99.95%, Smart Element; rest: >99%, Chempur) were purchased and used as received.

Melt synthesis of $\infty[\text{Ln}(\text{2-PyPz})_3]$, Ln = La, Ce, Pr, Nd, Sm, Eu, Gd, Tb, Dy, Ho (1–10): the freshly-filed respective rare earth metal (87.1 µmol) and a slight excess of 2-PyPzH ($\text{C}_8\text{H}_7\text{N}_3$, 275.5 µmol) were sealed under reduced pressure ($p = 1.0 \times 10^{-3}$ mbar) in an evacuated Duran® glass ampoule. The ampoule was heated to 200 °C within 48 h and maintained at this temperature for 120 h. The reaction mixture was then cooled to room temperature within 24 h. Excess Ln metal was not observed in any case and the excess ligand was washed away using dichloromethane (DCM).

Solvothermal synthesis of $\infty[\text{Ln}(\text{2-PyPz})_3]$, Ln = La, Ce, Pr, Nd, Sm, Eu, Gd, Tb, Dy, Ho (1–10): prepared as described for melt synthesis with addition of 0.3 m of pyridine before freezing with liquid nitrogen and sealing the ampoule. The temperature of the ampoule was raised to 240 °C within 72 h and maintained at this temperature for 96 h. The ampoule was then cooled to room temperature within 72 h. In $\infty[\text{Eu}(\text{2-PyPz})_3]$ (**6**), colorless block crystals were obtained and selected for SCXRD measurement.

$\infty[\text{La}(\text{2-PyPz})_3]$: $\text{C}_{24}\text{H}_{18}\text{N}_9\text{La}$ (571.36 g·mol^{−1}): C 49.51 (calcd. 50.45); H 3.30 (3.18); N 21.44 (22.06)%. Yield: 40 mg (80%). **FT-IR** (ATR): $\tilde{\nu}$ = 3070 (w), 1597 (m), 1565 (w), 1523 (w), 1454 (w), 1425 (m), 1342 (m), 1273 (w), 1152 (m), 1104 (w), 1083 (s), 1060 (w), 1003 (w), 969 (m), 935 (w), 852 (w), 788 (w), 755 (s), 709 (m), 656 (m), 631 (m), 511 (w), 467 (m) cm^{−1}.

$\infty[\text{Ce}(\text{2-PyPz})_3]$: $\text{C}_{24}\text{H}_{18}\text{N}_9\text{Ce}$ (572.58 g·mol^{−1}): C 49.81 (calcd. 50.34); H 3.26 (3.17); N 21.37 (22.02)%. Yield: 42 mg (84%). **FT-IR** (ATR): $\tilde{\nu}$ = 3065 (w), 1712 (w), 1596 (s), 1565 (m), 1524 (m), 1453 (m), 1425 (s), 1342 (m), 1273 (w), 1152 (m), 1127 (w), 1104 (w), 1083 (s), 1061 (m), 1003 (w), 969 (m), 935 (m), 788 (w), 755 (s), 709 (m), 656 (m), 630 (m), 513 (w), 468 (w) cm^{−1}.

$\infty[\text{Pr}(\text{2-PyPz})_3]$: $\text{C}_{24}\text{H}_{18}\text{N}_9\text{Pr}$ (573.37 g·mol^{−1}): C 49.39 (calcd. 50.27); H 3.07 (3.16); N 21.16 (21.99)%. Yield: 43 mg (85%). **FT-IR** (ATR): $\tilde{\nu}$ = 3088 (w), 1714 (w), 1597 (s), 1566 (m), 1525 (m), 1454 (m), 1425 (m), 1343 (m), 1273 (w), 1152 (m), 1104 (w), 1083 (s), 1061 (m), 1008 (w), 970 (m), 935 (m), 861 (w), 788 (w), 755 (s), 710 (m), 657 (m), 631 (m), 512 (w), 470 (m), 435 (m) cm^{−1}.

$\infty[\text{Nd}(\text{2-PyPz})_3]$: $\text{C}_{24}\text{H}_{18}\text{N}_9\text{Nd}$ (576.70 g·mol^{−1}): C 48.95 (calcd. 49.98); H 3.12 (3.15); N 20.98 (21.86)%. Yield: 41 mg (81%). **FT-IR** (ATR): $\tilde{\nu}$ = 3063 (w), 1713 (w), 1596 (m), 1565 (m), 1524 (m), 1454 (m), 1425 (m), 1343 (m), 1273 (w), 1151 (m), 1128 (w), 1104 (w), 1082 (s), 1061 (m), 1002 (w), 968 (m), 935 (m), 859 (w), 788 (w), 754 (s), 709 (m), 656 (m), 630 (m), 512 (w), 469 (m) cm^{−1}.

$\infty[\text{Sm}(\text{2-PyPz})_3]$: $\text{C}_{24}\text{H}_{18}\text{N}_9\text{Sm}$ (582.82 g·mol^{−1}): C 48.94 (calcd. 49.46); H 2.81 (3.11); N 21.52 (21.63)%. Yield: 48 mg (94%). **FT-IR** (ATR): $\tilde{\nu}$ = 3102 (w), 1714 (w), 1596 (m), 1566 (m), 1526 (m), 1454 (w), 1426 (m), 1344 (m), 1273 (w), 1152 (m), 1104 (w), 1082 (m), 1062 (w), 1002 (w), 970 (m), 935 (m), 859 (w), 788 (w), 754 (s), 710 (m), 657 (m), 630 (m), 513 (m), 472 (m) cm^{−1}.

$\infty[\text{Eu}(\text{2-PyPz})_3]$: $\text{C}_{24}\text{H}_{18}\text{N}_9\text{Eu}$ (584.42 g·mol^{−1}): C 48.80 (calcd. 49.32); H 3.05 (3.10); N 20.49 (21.57)%. Yield: 41 mg (82%). **FT-IR** (ATR): $\tilde{\nu}$ = 3075 (w), 1721 (w), 1598 (s), 1567 (m), 1527 (m), 1455 (m), 1427 (m), 1346 (m), 1274 (w), 1153 (m), 1129 (w), 1105 (m), 1084 (s), 1063 (m), 1009 (w), 972 (m), 936 (m), 862 (w), 789 (w), 757 (s), 711 (m), 659 (s), 631 (m), 516 (w), 473 (m) cm^{−1}.

$\infty[\text{Gd}(\text{2-PyPz})_3]$: $\text{C}_{24}\text{H}_{18}\text{N}_9\text{Gd}$ (589.71 g·mol^{−1}): C 49.74 (calcd. 48.88); H 2.32 (3.08); N 20.34 (21.38)%. Yield: 45 mg (88%). **FT-IR** (ATR): $\tilde{\nu}$ = 3067 (w), 1720 (w), 1597 (s), 1566 (m), 1527 (m), 1454 (m), 1426 (m), 1345 (m), 1273 (w), 1152 (m), 1104 (w), 1082 (s), 1062 (m), 967 (m), 935 (m), 861 (w), 788 (w), 754 (s), 710 (m), 658 (m), 629 (m), 514 (w), 473 (m) cm^{−1}.

$\infty[\text{Tb}(\text{2-PyPz})_3]$: $\text{C}_{24}\text{H}_{18}\text{N}_9\text{Tb}$ (591.38 g·mol^{−1}): C 49.36 (calcd. 48.74); H 2.67 (3.07); N 22.1 (21.32)%. Yield: 43 mg (83%). **FT-IR** (ATR): $\tilde{\nu}$ = 3065 (w), 1723 (w), 1597 (s), 1567 (m), 1528 (m), 1455 (w), 1426 (m), 1346 (m), 1274 (w), 1152 (m), 1104 (w), 1082 (s), 1062 (w), 1010 (w), 968 (m), 935 (m), 863 (w), 788 (w), 755 (s), 710 (m), 658 (m), 629 (m), 513 (w), 473 (m) cm^{−1}.

$\infty[\text{Dy}(\text{2-PyPz})_3]$: $\text{C}_{24}\text{H}_{18}\text{N}_9\text{Dy}$ (594.96 g·mol^{−1}): C 48.75 (calcd. 48.45); H 3.32 (3.05); N 20.77 (21.19)%. Yield: 44 mg (85%). **FT-IR** (ATR): $\tilde{\nu}$ = 3098 (w), 1722 (m), 1597 (m), 1566 (w), 1528 (w), 1454 (w), 1426 (m), 1346 (m), 1274 (w), 1151 (w), 1104 (w), 1081 (m), 1062 (w), 1010 (w), 967 (m), 935 (w), 864 (w), 788 (w), 754 (s), 710 (m), 658 (m), 629 (w), 514 (w), 474 (m) cm^{−1}.

$\infty[\text{Ho}(\text{2-PyPz})_3]$: $\text{C}_{24}\text{H}_{18}\text{N}_9\text{Ho}$ (597.39 g·mol^{−1}): C 49.14 (calcd. 48.25); H 3.84 (3.04); N 20.69 (21.10)%. Yield: 40 mg (77%). **FT-IR** (ATR): $\tilde{\nu}$ = 2988 (w), 1728 (w), 1599 (s), 1567 (m), 1530 (m), 1455 (m), 1428 (s), 1348 (m), 1274 (w), 1152 (w), 1082 (s), 1063 (m), 1010 (w), 986 (m), 936 (w), 867 (w), 789 (w), 757 (s), 711 (m), 660 (m), 631 (w), 515 (w), 478 (m), 430 (m) cm^{−1}.

Synthesis of $\infty[\text{Ce}_{1-x}\text{Tb}_x(\text{2-PyPz})_3]$ (2a**, **2b**), $\infty[\text{Tb}_{0.90}\text{Ce}_{0.1}(\text{2-PyPz})_3]$ (**8a**):** By mixing and grinding Ce metal in a mortar with 0.5% Tb (**2a**), 5% Tb (**2b**) and the other way around with 10% Ce (**8a**) for the synthesis of three co-doped samples differing in Ln content. 87.1 µmol of the mixture was placed in an ampoule, where the reaction was carried out under the same heating conditions as described above.

Synthesis of $\infty[\text{Gd}_{1-x-y}\text{Eu}_x\text{Tb}_y(\text{2-PyPz})_3]$: Eu^{3+} , Tb^{3+} (7a–7f**):** Six ratios were synthesized with 0.2% Eu (**7a**), 0.3% Eu (**7b**), 0.5% Eu (**7c**), 1% Eu (**7d**), 1% Eu with 1% Tb (**7e**), and 1% Tb (**7f**). The required amounts of the freshly filed metals (87.1 µmol) were mixed and ground in a mortar to acquire the best homogeneity. Reactions

were carried out under the same heating conditions as previously described.

Synthesis of $^1_{\infty}[\text{Eu}_{1-x}\text{Tb}_x(2\text{-PyPz})_3]$ (6a–6c), $^1_{\infty}[\text{Tb}_{0.95}\text{Eu}_{0.05}(2\text{-PyPz})_3]$ (8b): a ratio of 5% (6a), 25% (6b), 50% (6c), 95% (8b) Tb was ground together with freshly filed Eu to achieve the best homogeneity. The reaction was carried out as previously described.

Synthesis of $[\text{Tb}_2\text{Ca}(2\text{-PyPz})_8]$ (11): Tb metal filing (66.1 μmol), calcium metal (33.2 μmol) and 2-PyPzH ($\text{C}_8\text{H}_7\text{N}_3$, 265.6 μmol) in the presence of 0.2 ml of pyridine were sealed in an evacuated ampoule. Before applying a vacuum to the ampoule as well as for sealing the ampoule, the solvent was frozen using liquid nitrogen. The reaction mixture was heated to 180 °C in 24 h, the temperature was raised again to 200 °C in 48 h and maintained at this temperature for 72 h. The ampoule was cooled to room temperature over a further 72 h. Plate crystals were selected for the SCXRD measurement. $\text{C}_{64}\text{H}_{48}\text{N}_{24}\text{CaTb}_2$ (1511.15 $\text{g}\cdot\text{mol}^{-1}$): C 49.50 (calcd. 50.87); H 3.09 (3.20); N 21.61 (22.25)%. Yield: 53 mg (78%). **FT-IR** (ATR): $\tilde{\nu}$ = 3080 (w), 1716 (w), 1601 (s), 1564 (m), 1531 (m), 1458 (m), 1423 (m), 1342 (m), 1278 (m), 1156 (m), 1126 (w), 1106 (m), 1088 (s), 1057 (m), 1005 (m), 971 (m), 939 (w), 861 (w), 790 (w), 754 (s), 710 (w), 702 (w), 653 (m), 635 (m), 509 (w), 470 (m) cm^{-1} .

Synthesis of $[\text{Tb}_2\text{AE}(2\text{-PyPz})_8]$, AE = Sr (12), Ba (13): A mixture of freshly-filed Tb (62.2 μmol), pieces of the respective AE metal (31.0 μmol), and 2-PyPzH ($\text{C}_8\text{H}_7\text{N}_3$, 248 μmol), in 0.6 ml pyridine was sealed in an evacuated DURAN glass ampoule. Before applying a vacuum to the ampoule as well as for sealing the ampoule, the solvent was frozen with liquid nitrogen. The oven was heated to 180 °C in 1 h. Subsequently, the temperature was raised to 205 °C in 24 h. The temperature was held for 96 h and then lowered to room temperature over a further 24 h. Colorless crystals were selected for SCXRD measurements.

$[\text{Tb}_2\text{Sr}(2\text{-PyPz})_8]$: $\text{C}_{64}\text{H}_{48}\text{N}_{24}\text{SrTb}_2$ (1558.70 $\text{g}\cdot\text{mol}^{-1}$): C 49.04 (calcd. 49.32); H 3.18 (3.10); N 20.68 (21.57)%. Yield: 44 mg (75%). **FT-IR** (ATR): $\tilde{\nu}$ = 3076 (w), 1715 (w), 1599 (s), 1563 (m), 1529 (m), 1454 (m), 1424 (m), 1349 (w), 1333 (m), 1276 (m), 1151 (w), 1108 (w), 1087 (m), 1074 (w), 1052 (w), 1005 (w), 969 (w), 939 (w), 878 (w), 788 (w), 757 (s), 710 (m), 653 (m), 634 (m), 510 (m), 468 (w) cm^{-1} .

$[\text{Tb}_2\text{Ba}(2\text{-PyPz})_8]$: $\text{C}_{64}\text{H}_{48}\text{N}_{24}\text{BaTb}_2$ (1608.40 $\text{g}\cdot\text{mol}^{-1}$): C 46.66 (calcd. 47.79); H 3.19 (3.01); N 20.05 (20.90)%. Yield: 35 mg (79%). **FT-IR** (ATR): $\tilde{\nu}$ = 3075 (w), 1712 (w), 1599 (m), 1563 (w), 1529 (m), 1453 (m), 1421 (w), 1347 (w), 1333 (w), 1275 (w), 1152 (w), 1124 (w), 1106 (w), 1087 (m), 1071 (w), 1052 (w), 1005 (w), 968 (w), 937 (w), 927 (w), 878 (w), 860 (w), 788 (w), 758 (s), 710 (w), 700 (w), 652 (w), 633 (m), 510 (w), 468 (w) cm^{-1} .

Synthesis of $[\text{AE}(2\text{-PyPz})_2(2\text{-PyPzH})_2]$, AE = Ca (14), Sr (15): Pieces of the respective AE metal or even CaCl_2 (68.8 μmol) and a slight excess of 2-PyPzH ($\text{C}_8\text{H}_7\text{N}_3$, 289.3 μmol) together with 0.3 ml pyridine were sealed in an evacuated ampoule. Before applying a vacuum to the ampoule as well as for sealing the ampoule, the solvent was frozen with liquid nitrogen. The ampoule was heated to 180 °C in 24 h and then 200 °C in 48 h. The temperature was held for 72 h and then lowered to 25 °C in another 24 h. Colorless single crystals were separated. The excess ligand was washed using DCM.

$[\text{Ca}(2\text{-PyPz})_2(2\text{-PyPzH})_2]$: $\text{C}_{32}\text{H}_{26}\text{N}_{12}\text{Ca}$ (618.71 $\text{g}\cdot\text{mol}^{-1}$): C 61.32 (calcd. 62.21); H 4.01 (4.24); N 26.50 (27.17)%. Yield: 35 mg (82%). **FT-IR** (ATR): $\tilde{\nu}$ = 3084 (w), 1698 (s), 1567 (m), 1515 (m), 1446 (w), 1428 (m), 1357 (w), 1341 (w), 1307 (w), 1281 (w), 1244 (w), 1223 (m), 1195 (w), 1156 (m), 1081 (m), 1052 (m), 1001 (m), 961 (m), 855 (w), 793 (w), 754 (s), 701 (m), 651 (w), 630 (m), 512 (w), 466 (m), 436 (m) cm^{-1} .

$[\text{Sr}(2\text{-PyPz})_2(2\text{-PyPzH})_2]$: $\text{C}_{32}\text{H}_{26}\text{N}_{12}\text{Sr}$ (666.25 $\text{g}\cdot\text{mol}^{-1}$): C 56.66 (calcd. 57.69); H 4.68 (3.93); N 24.50 (25.23)%. Yield: 38 mg (83%). **FT-IR**

(ATR): $\tilde{\nu}$ = 3091 (w), 1596 (s), 1565 (w), 1512 (m), 1445 (w), 1428 (m), 1339 (w), 1307 (w), 1278 (w), 1222 (w), 1154 (m), 1083 (m), 1050 (m), 1000 (w), 961 (m), 793 (w), 757 (s), 708 (m), 630 (m), 513 (w), 501 (w), 463 (w), 442 (w) cm^{-1} .

Acknowledgments

The authors acknowledge DESY (Hamburg, Germany), a member of the Helmholtz Association HGF, for providing experimental facilities. Parts of this research were carried out at PETRA III, and we thank Carsten Paulmann and Heiko Schulz-Ritter for assistance in using beamline P24, beamtime allocated for proposal I-20180762. In addition, we gratefully acknowledge the support of the Volkswagen Foundation within the project "Molecular materials – bridging magnetism and luminescence". H. Youssef gratefully acknowledges the Egyptian Ministry of Higher Education (MoHE) and the German Academic Exchange Service (DAAD) under the German Egyptian Research Long-term Scholarship (GERLS) Programme, 2017 (57311832) for a Ph.D. fellowship. I. V. Taydakov gratefully acknowledges the Russian Science Foundation (project N° 19-13-00272) for financial support. Open Access funding enabled and organized by Projekt DEAL.

Conflict of Interest

The authors declare no conflict of interest.

Data Availability Statement

The data that support the findings of this study are available in the supplementary material of this article.

Keywords: Cerium • Alkaline earth metals • Luminescence • Heterobimetallic • melt synthesis

- [1] a) Y. Yuan, D. Wang, B. Zhou, S. Feng, M. Sun, S. Zhang, W. Gao, Y. Bi, H. Qin, *Opt. Mater. Express* **2018**, *8*, 2760–2767; b) G. Fasol, *Science* **1997**, *275*, 941–942; c) Y. Wang, L. Wang, S. Bao, L. Xu, J. Zhang, Y. Liang, L. Wang, X. Liang, W. Xiang, *J. Alloys Compd.* **2022**, *921*, 166083.
- [2] a) Q.-Q. Zhu, Y. Meng, H. Zhang, S. Li, L. Wang, R.-J. Xie, *ACS Appl. Electron. Mater.* **2020**, *2*, 2644–2650; b) S. Bao, Y. Liang, L. Wang, L. Wang, L. Xu, Y. Wang, X. Liang, W. Xiang, *ACS Sustainable Chem. Eng.* **2022**, *10*, 8105–8114; c) T. Long, Z. Wang, Y. Fan, H. Lin, H. Sun, C. Zou, D. Zhang, S. Zhuang, *Ceram. Int.* **2022**, *48*, 16391–16396.
- [3] a) H. Yin, P. J. Carroll, J. M. Anna, E. J. Schelter, *J. Am. Chem. Soc.* **2015**, *137*, 9234–9237; b) Y. Qiao, D.-C. Sergentu, H. Yin, A. V. Zabula, T. Cheisson, A. McSkimming, B. C. Manor, P. J. Carroll, J. M. Anna, J. Autschbach, E. J. Schelter, *J. Am. Chem. Soc.* **2018**, *140*, 4588–4595; c) P. Lindqvist-Reis, F. Réal, R. Janicki, V. Vallet, *Inorg. Chem.* **2018**, *57*, 10111–10121.
- [4] a) L. Wang, Z. Zhao, G. Zhan, H. Fang, H. Yang, T. Huang, Y. Zhang, N. Jiang, L. Duan, Z. Liu, Z. Bian, Z. Lu, C. Huang, *Light-*

- Sci. Appl.* **2020**, *9*, 1–9; b) Z. Zhao, L. Wang, G. Zhan, Z. Liu, Z. Bian, C. Huang, *Natl. Sci. Rev.* **2021**, *8*, nwaa193.
- [5] a) L. V. Meyer, F. Schönfeld, A. Zurawski, M. Mai, C. Feldmann, K. Müller-Buschbaum, *Dalton Trans.* **2015**, *44*, 4070–4079; b) X. Qin, X. Liu, W. Huang, M. Bettinelli, X. Liu, *Chem. Rev.* **2017**, *117*, 4488–4527; c) P. R. Matthes, K. Müller-Buschbaum, *Z. Anorg. Allg. Chem.* **2014**, *640*, 2847–2851; d) H. Yin, P. J. Carroll, B. C. Manor, J. M. Anna, E. J. Schelter, *J. Am. Chem. Soc.* **2016**, *138*, 5984–5993.
- [6] O. S. Wenger, *J. Am. Chem. Soc.* **2018**, *140*, 13522–13533.
- [7] S. T. Frey, W. D. Horrocks Jr., *Inorg. Chem.* **1991**, *30*, 1073–1079.
- [8] a) G. Blasse, B. C. Grabmaier, in *A general introduction to luminescent materials*, Springer Berlin, **1994**, pp. 1–9; b) P. Fang, L. Wang, G. Zhan, W. Yan, P. Huo, A. Ying, Y. Zhang, Z. Zhao, G. Yu, Y. Huang, S. Gong, L. Duan, Z. Liu, Z. Bian, C. Huang, *ACS Appl. Mater. Interfaces* **2021**, *13*, 45686–45695.
- [9] a) N. Kodama, Y. Tani, M. Yamaga, *J. Lumin.* **2000**, *87*, 1076–1078; b) G. C. Kim, H. L. Park, S. I. Yun, B. G. Moon, *J. Mater. Sci. Lett.* **1986**, *5*, 359–360; c) J. W. H. Van Krevel, H. T. Hintzen, R. Metselaar, A. Meijerink, *J. Alloys Compd.* **1998**, *268*, 272–277; d) G. Gauthier, S. Jobic, M. Evain, H.-J. Koo, M.-H. Whangbo, C. Fouassier, R. Brec, *Chem. Mater.* **2003**, *15*, 828–837.
- [10] G. Blasse, A. Bril, *Appl. Phys. Lett.* **1967**, *11*, 53–55.
- [11] a) D. Wu, Z. Hao, X. Zhang, G.-H. Pan, Y. Luo, L. Zhang, H. Zhao, J. Zhang, *J. Lumin.* **2017**, *186*, 170–174; b) J. M. Ogiegło, A. Zych, T. Jüstel, A. Meijerink, C. R. Ronda, *Opt. Mater.* **2013**, *35*, 322–331.
- [12] a) D. A. I. Peng, J. I. Cheng, S. H. E. N. Liming, Q. I. A. N. Qi, G. U. O. Guobiao, X. Zhang, B. A. O. Ningzhong, *J. Rare Earth* **2017**, *35*, 341–346; b) P. Zeng, X. Wei, S. Zhou, M. Yin, Y. Chen, *J. Appl. Phys.* **2016**, *120*, 093104.
- [13] R. M. Kowalski, J. Komar, P. Solarz, *J. Alloys Compd.* **2020**, *848*, 156228.
- [14] S. Chawla, T. Roy, K. Majumder, A. Yadav, *J. Exp. Nanosci.* **2014**, *9*, 776–784.
- [15] a) T. Hasegawa, S. W. Kim, T. Ueda, T. Ishigaki, K. Uematsu, H. Takaba, K. Toda, M. Sato, *J. Mater. Chem. C* **2017**, *5*, 9472–9478; b) Y. Wang, J. Ding, Z. Zhao, Y. Wang, *Inorg. Chem.* **2018**, *57*, 14542–14553.
- [16] a) Y. Chen, L. Li, Q. Zhang, S. Liu, Z. Tian, Z. Ju, *J. Solid State Chem.* **2020**, *281*, 121053; b) E. Bartolomé, A. Arauzo, J. Luzón, S. Melnic, S. Shova, D. Prodius, J. Bartolomé, A. Amann, M. Nallaiyan, S. Spagna, *Dalton Trans.* **2019**, *48*, 5022–5034; c) B. D. Chandler, D. T. Cramb, G. K. H. Shimizu, *J. Am. Chem. Soc.* **2006**, *128*, 10403–10412.
- [17] G. B. Deacon, P. C. Junk, S. G. Leary, A. Urbatsch, *Z. Anorg. Allg. Chem.* **2012**, *638*, 2001–2007.
- [18] Y. Chen, Q. Gao, D. Gao, D. Wang, Y. Li, W. Liu, W. Li, *J. Coord. Chem.* **2013**, *66*, 3829–3838.
- [19] a) K. Singh, J. R. Long, P. Stavropoulos, *J. Am. Chem. Soc.* **1997**, *119*, 2942–2943; b) A. C. Coelho, M. Nolasco, S. S. Balula, M. M. Antunes, C. C. L. Pereira, F. A. Almeida Paz, A. A. Valente, M. Pillinger, P. Ribeiro-Claro, J. Klinowski, I. S. Gonçalves, *Inorg. Chem.* **2011**, *50*, 525–538; c) T. L. Hu, J. R. Li, C. S. Liu, X. S. Shi, J. N. Zhou, X. H. Bu, J. Ribas, *Inorg. Chem.* **2006**, *45*, 162–173; d) P. L. Jones, J. C. Jeffery, J. A. McCleverty, M. D. Ward, *Polyhedron* **1997**, *16*, 1567–1571; e) S. Sethi, S. Jena, P. K. Das, N. Behera, *J. Mol. Struct.* **2019**, *1193*, 495–521.
- [20] a) R. Q. Zou, X. H. Bu, M. Du, Y. X. Sui, *J. Mol. Struct.* **2004**, *707*, 11–15; b) Y. Zhang, D. Zhao, Z. Liu, J. Yang, X. Niu, L. Fan, T. Hu, *J. Solid State Chem.* **2020**, *282*, 121086; c) D. Ma, L. Duan, Y. Wei, Y. Qiu, *Chem. Eur. J.* **2014**, *20*, 15903–15912; d) J. Abbeneth, M. Diefenbach, A. Hinz, L. Alig, C. Würtele, J. M. Goicoechea, M. C. Holthausen, S. Schneider, *Angew. Chem. Int. Ed.* **2019**, *58*, 10966–10970; *Angew. Chem.* **2019**, *131*, 11082–11086; e) L. Fan, F. Wang, D. Zhao, X. Sun, H. Chen, H. Wang, X. Zhang, *Spectrochim. Acta Part A* **2020**, *239*, 118467; f) L. He, L. Duan, J. Qiao, D. Zhang, L. Wang, Y. Qiu, *Chem. Commun.* **2011**, *47*, 6467–6469; g) C.-S. Liu, J.-J. Wang, Z. Chang, L.-F. Yan, X.-H. Bu, *CrystEngComm* **2010**, *12*, 1833–1841; h) T.-L. Hu, R.-Q. Zou, J.-R. Li, X.-H. Bu, *Dalton Trans.* **2008**, *10*, 1302–1311; i) J.-J. Wang, C.-S. Liu, T.-L. Hu, Z. Chang, C.-Y. Li, L.-F. Yan, P.-Q. Chen, X.-H. Bu, Q. Wu, L.-J. Zhao, Z. Wang, X.-Z. Zhang, *CrystEngComm* **2008**, *10*, 681–692.
- [21] R. Q. Zou, X. H. Bu, R. H. Zhang, *Inorg. Chem.* **2004**, *43*, 5382–5386.
- [22] D. Su, Y. Liu, S. Li, S. Ding, Y. Jin, Z. Wang, X. Hu, L. Zhang, *Eur. J. Inorg. Chem.* **2017**, *2017*, 651–658.
- [23] a) T. J. Sherbow, J. C. Fetting, L. A. Berben, *Inorg. Chem.* **2017**, *56*, 8651–8660; b) C. M. Pask, S. Greatorex, R. Kulmaczewski, A. Baldansuren, E. J. McInnes, F. Bamiduro, M. Yamada, N. Yoshinari, T. Konno, M. A. Halcrow, *Chem. Eur. J.* **2020**, *26*, 4833–4841; c) Y. Pankratova, D. Aleshin, I. Nikovskiy, V. Novikov, Y. Nelyubina, *Inorg. Chem.* **2020**, *59*, 7700–7709; d) N. S. Labrum, M. Pink, C.-H. Chen, K. G. Caulton, *Eur. J. Inorg. Chem.* **2019**, *2019*, 1932–1940; e) E. Coronado, J. R. G. Mascarós, M. C. Giménez-López, M. Almeida, J. C. Waerenborgh, *Polyhedron* **2007**, *26*, 1838–1844.
- [24] a) N. Du, X. Gao, J. Song, Z.-N. Wang, Y.-H. Xing, F.-Y. Bai, Z. Shi, *RSC Adv.* **2016**, *6*, 71012–71024; b) M. H. W. Lam, D. Y. K. Lee, S. S. M. Chiu, K. W. Man, W. T. Wong, *Eur. J. Inorg. Chem.* **2000**, *2000*, 1483–1488; c) L. Norel, L. E. Darago, B. Le Guennic, K. Chakarawet, M. I. Gonzalez, J. H. Olshansky, S. Rigaut, J. R. Long, *Angew. Chem. Int. Ed.* **2018**, *57*, 1933–1938; *Angew. Chem.* **2018**, *130*, 1951–1956; d) G. M. Davies, H. Adams, S. J. A. Pope, S. Faulkner, M. D. Ward, *Photochem. Photobiol. Sci.* **2005**, *4*, 829–834; e) Y.-W. Yip, H. Wen, W.-T. Wong, P. A. Tanner, K.-L. Wong, *Inorg. Chem.* **2012**, *51*, 7013–7015.
- [25] a) E. Psillakis, J. C. Jeffery, J. A. McCleverty, M. D. Ward, *J. Chem. Soc. Dalton Trans.* **1997**, *9*, 1645–1651; b) B. Schowtka, H. Görls, M. Westerhausen, *Z. Anorg. Allg. Chem.* **2015**, *641*, 650–654; c) T. Kloubert, C. Müller, S. Kriek, T. Schlotthauer, H. Görls, M. Westerhausen, *Eur. J. Inorg. Chem.* **2012**, *2012*, 5991–6001.
- [26] L.-R. Xing, Z. Lu, M. Li, J. Zheng, D. Li, *J. Phys. Chem. Lett.* **2020**, *11*, 2067–2073.
- [27] H. Youssef, A. E. Sedykh, J. Becker, T. Schäfer, I. V. Taydakov, H. R. Li, K. Müller-Buschbaum, *Chem. Eur. J.* **2021**, *27*, 16634–16641.
- [28] C. Müller, A. Koch, H. Görls, S. Kriek, M. Westerhausen, *Inorg. Chem.* **2015**, *54*, 635–645.
- [29] a) D. J. Lewis, F. Moretta, A. T. Holloway, Z. Pikramenou, *Dalton Trans.* **2012**, *41*, 13138–13146; b) M. Mahato, P. P. Jana, K. Harms, H. P. Nayek, *RSC Adv.* **2015**, *5*, 62167–62172; c) C. Y. Chow, S. V. Eliseeva, E. R. Trivedi, T. N. Nguyen, J. W. Kampf, S. Petoud, V. L. Pecoraro, *J. Am. Chem. Soc.* **2016**, *138*, 5100–5109.
- [30] a) P. R. Sathees Chandran, U. S. Soumya Mol, R. Drisya, M. R. Sudarsanakumar, M. R. Prathapachandra Kurup, *J. Mol. Struct.* **2017**, *1137*, 396–402; b) X. Zhou, H. Wang, S. Jiang, G. Xiang, X. Tang, X. Luo, L. Li, X. Zhou, *Inorg. Chem.* **2019**, *58*, 3780–3788; c) M. Hasegawa, H. Ohtsu, D. Kodama, T. Kasai, S. Sakurai, A. Ishii, K. Suzuki, *New J. Chem.* **2014**, *38*, 1225–1234; d) C. Seidel, C. Lorbeer, J. Cybińska, A.-V. Mudring, U. Ruschewitz, *Inorg. Chem.* **2012**, *51*, 4679–4688.
- [31] C. S. Liu, X. S. Shi, J. R. Li, J. J. Wang, X. H. Bu, *Cryst. Growth Des.* **2006**, *6*, 656–663.
- [32] a) W. T. Carnall, P. R. Fields, K. Rajnak, *J. Chem. Phys.* **1968**, *49*, 4424–4442; b) W. T. Carnall, P. R. Fields, K. Rajnak, *J. Chem. Phys.* **1968**, *49*, 4450–4455; c) W. T. Carnall, P. R. Fields, K. Rajnak, *J. Chem. Phys.* **1968**, *49*, 4447–4449; d) E. Huskowska, I. Turowska-Tyrk, J. Legendziewicz, J. P. Riehl, *New J. Chem.* **2002**, *26*, 1461–1467.

- [33] a) P. Wang, R.-Q. Fan, Y.-L. Yang, X.-R. Liu, P. Xiao, X.-Y. Li, W. Hasi, W.-W. Cao, *CrystEngComm* **2013**, *15*, 4489–4506; b) P. Wang, R.-Q. Fan, X.-R. Liu, L.-Y. Wang, Y.-L. Yang, W.-W. Cao, B. Yang, W. Hasi, Q. Su, Y. Mu, *CrystEngComm* **2013**, *15*, 1931–1949; c) A. E. Sedykh, D. G. Kurth, K. Müller-Buschbaum, *Eur. J. Inorg. Chem.* **2019**, 2019, 4564–4571.
- [34] a) M. H. V. Werts, R. T. F. Jukes, J. W. Verhoeven, *Phys. Chem. Chem. Phys.* **2002**, *4*, 1542–1548; b) A. Aebischer, F. Gumy, J.-C. G. Bünzli, *Phys. Chem. Chem. Phys.* **2009**, *11*, 1346–1353.
- [35] a) K. Binnemans, *Coord. Chem. Rev.* **2015**, *295*, 1–45; b) K. Binnemans, *Chem. Rev.* **2009**, *109*, 4283–4374.
- [36] H. A. A. Seed Ahmed, O. M. Ntwaeaborwa, R. E. Kroon, *Curr. Appl. Phys.* **2013**, *13*, 1264–1268.
- [37] P. R. Matthes, C. J. Höller, M. Mai, J. Heck, S. J. Sedlmaier, S. Schmiechen, C. Feldmann, W. Schnick, K. Müller-Buschbaum, *J. Mater. Chem.* **2012**, *22*, 10179–10187.
- [38] a) A. J. Amoroso, A. M. C. Thompson, J. C. Jeffery, P. L. Jones, J. A. McCleverty, M. D. Ward, *J. Chem. Soc. Chem. Commun.* **1994**, *24*, 2751–2752; b) J. Salinas Uber, Y. Vogels, D. van den Helder, I. Mutikainen, U. Turpeinen, W. T. Fu, O. Roubeau, P. Gamez, J. Reedijk, *Eur. J. Inorg. Chem.* **2007**, *26*, 4197–4206

Manuscript received: September 7, 2022

Revised manuscript received: November 3, 2022

Accepted manuscript online: November 22, 2022
